Atmospheric Environment 45 (2011) 594–604

Contents lists available at ScienceDirect

Atmospheric Environment

journal homepage: www.elsevier.com/locate/atmosenv

Transport pathways and potential sources of PM_{10} in Beijing

Lei Zhu, Xin Huang, Hui Shi, Xuhui Cai, Yu Song*

State Key Joint Laboratory of Environmental Simulation and Pollution Control, Department of Environmental Science, Peking University, Beijing 100871, China

ARTICLE INFO

Article history:
Received 18 April 2010
Received in revised form
20 October 2010
Accepted 25 October 2010

Keywords:
Transport pathway
Backward trajectory
Trajectory cluster
Trajectory sector analysis (TSA)
Potential source contribution function (PSCF)

ABSTRACT

Beijing has suffered from major air pollution in recent years from PM_{10}. In this study, we investigated the transport pathways and potential sources of PM_{10} concentration based on backward trajectories and PM_{10} concentration records from 2003 to 2009. Four transport pathways of high PM_{10} existed. One was the northwest pathway, which had the most frequency of occurrence in spring and winter, and traveled over the southern Mongolia, western Inner Mongolia, and Loess plateaus. The second one was the south pathway, which mostly occurred during May and September, and passed from the south of Beijing. The third one was the V-shape southwest pathway, which occurred mostly during early autumn and passed over the west and south of Hebei. The highest PM_{10} concentration was found with the southwest pathway, which occurs mostly in April and October, and traveled over the Loess Plateau and the west and south of Hebei. Low concentrations of PM_{10} with the southwest and east pathways were possible due to intensive precipitation in summer. Characterizing with the lowest PM_{10} concentration, the north pathway was possible associated with strong winds that leaded to diffusion of air pollutants in Beijing. The contribution of PM_{10} from long transported was about 39.3 $\mu g\ m^{-3}$, which accounted for about 26.0% of the PM_{10} concentrations in Beijing.

1. Introduction

Particulate matter with aerodynamic diameters smaller than 10 μm (PM_{10}) was found to be harmful to human health (Schwartz et al., 1996; Ostro et al., 2006). Beijing, a mega city, drew much attention from researchers due to its air pollution (Chan and Yao, 2008; Parrish et al., 2009). PM_{10} is the major pollutant in Beijing. Its annual average concentrations from 2000 to 2008 were 162, 165, 166, 141, 149, 142, 161, 148, and 122 $\mu g\ m^{-3}$, respectively (Beijing Environmental Protection Bureau annual reports, 2000–2008). These concentrations exceeded the national second-class air-quality standard of 100 $\mu g\ m^{-3}$ for PM_{10} in China and the guideline of 20 $\mu g\ m^{-3}$ recommended by the World Health Organization (WHO, 2006).

Effective PM_{10} control strategies in Beijing require knowledge of transport pathways and potential sources of PM_{10}, and methods based on trajectories analysis had been commonly applied to this problem. Cluster analysis (Moody and Galloway, 1988; Borge et al., 2007) and trajectory sector analysis (TSA) (Parekh and Husain, 1982) can be used to identify transport pathways. Potential source contribution function (PSCF) (Ashbaugh et al., 1985) was used to investigate potential sources. However, little research had been done in Beijing based on these methods. Wang et al. (2004) used trajectory clustering and PSCF to identify three principal transport pathways for high-concentration PM_{10} in Beijing. Their study, focused on PM_{10} pollution solely during springtime, only considered a 3-year data set from 2001 to 2003.

In this study, we investigated transport pathways and potential sources of PM_{10} in urban Beijing for all seasons over a continuous 7-year data set from 2003 to 2009 by using multiple methods, including trajectory clustering, TSA, and PSCF.

2. Data and methods

2.1. PM_{10} data

The daily PM_{10} Air Pollution Index (API) (from noon to noon) data at two rural sites, two suburban sites and eight urban sites (Fig. 1a, b) from 2003 to 2009 were obtained from the Beijing Environmental Protection Bureau (BJEPB) Web site (BJEPB, 2003–2009). The API values were converted to PM_{10} concentrations using the API equations. The PM_{10} concentration was treated as missing when the primary pollutant was not PM_{10}. Moreover, a PM_{10} concentration of 600 $\mu g\ m^{-3}$ was assigned to events when the API equaled 500, which only accounted for 0.12% of the total data in the seven years. The missing data made up 6% of the total.

Daily PM_{10} concentration in the urban areas of Beijing was calculated by averaging concentrations from the eight urban

* Corresponding author.
E-mail address: songyu@pku.edu.cn (Y. Song).

1352-2310/$ – see front matter © 2010 Elsevier Ltd. All rights reserved.
doi:10.1016/j.atmosenv.2010.10.040

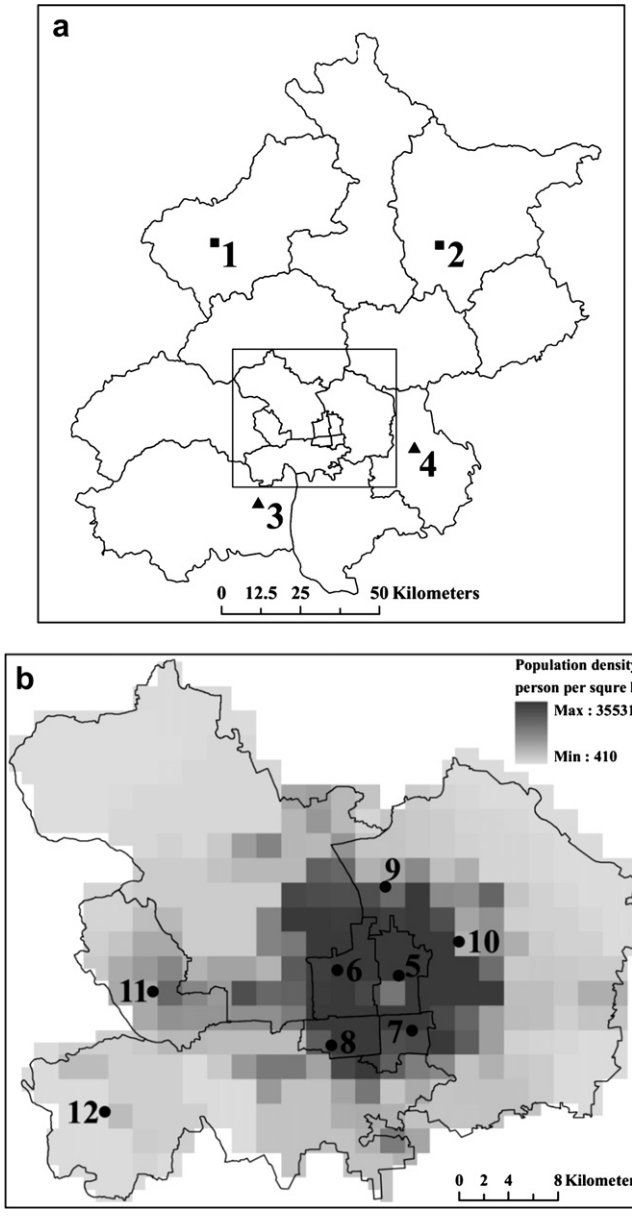

Fig. 1. (a) Two rural sites (squares): Yanqing (1) and Miyun (2), Two suburban sites (triangles): Tongzhou (3) and Fangshan (4); (b) Eight urban stations (dots): Dongsi (5), Guanyuan (6), Tiantan (7), Wanshouxigong (8), Aotizhongxin (9), Nongzhanguan (10), Yungang (11) and Gucheng (12). The limit of panel (b) is the inner rectangle in panel (a). Population density data (2 km resolution) in urban areas was of the year 2000.

stations. Seasonal average concentrations of PM_{10} from 2003 to 2009 were illustrated in Fig. 2. High PM_{10} concentrations in Beijing always occurred in the spring (March, April, and May), followed by autumn (September, October, and November) and winter (December, January, and February), then summer (June, July, and August).

2.2. Backward trajectory modeling

Backward trajectories were calculated using the HYSPLIT_4 (Hybrid Single-Particle Lagrangian Integrated Trajectory, Version 4) model (Roland and Hess, 2004) with NCEP/NCAR (National Centers for Environmental Prediction NCEP/National Center for Atmospheric Research) Global Reanalysis meteorological data. The reanalysis data

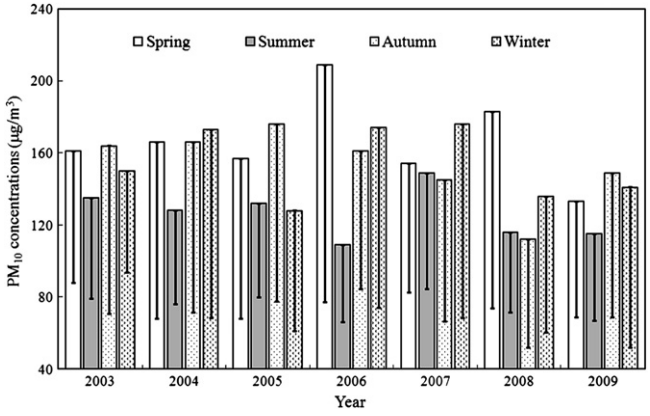

Fig. 2. Seasonal average concentrations of PM_{10} in the urban areas of Beijing from 2003 to 2009. Error bar illustrates the standard deviation of PM_{10} concentrations.

was available at every 6 h on the surface and at mandatory 17 pressure levels from 10 to 1000 hPa (http://ready.arl.noaa.gov/gbl_reanalysis.php).

Beijing experiences high PM_{10} pollution during spring dust storms. The typical wind speed of such dust storms is approximately 7 m s^{-1} or more, and the sand and dust sources are located about 1000–2000 km northwest of Beijing. Thus it usually takes less than 70 h for dust storms to reach Beijing. Using a backward trajectory length of 72 h was therefore reasonable for capturing such dust storms.

We used several receptor heights, i.e., 100, 200, 300, 500, and 1000 m, to study the transport pathways using the clustering method. However, no significant differences were found among the results except that the lengths of trajectories could increase with receptor height. We selected 200 m as the receptor height for the following reasons. First, PM_{10} concentrations are often measured below the surface layer, typically at 200 m, and pollutants within this layer are well mixed. Second, both horizontal and vertical advections were considered when calculating the backward trajectories (Roland and Hess, 2004). Air masses from higher or lower heights could thus reach the 200 m receptor height.

Backward trajectories started from the center of Beijing (39°54′27″N, 116°23′17″E) at 00:00, 06:00, 12:00, and 18:00 UTC each day. In total, 10,204 trajectories were generated throughout the study period. Although 6-h PM_{10} concentrations are generally preferable, using the 24-h average for each of the four 6-h periods still yielded representative results. Using a statistically robust number of trajectories was important to minimize errors (Qureshi et al., 2006).

2.3. Trajectory cluster method

As latitude increases, distances in the west-east direction decrease relative to longitude. To avoid this issue, we converted latitude and longitude into x, y distances in Cartesian coordinate, which were later used as clustering variables. Other studies have also applied this type of conversion (Cape et al., 2000; Riccio et al., 2007).

A two-stage clustering procedure (Davis, 1991; Eder et al., 1994; Oanh et al., 2005) was used to produce clusters. In the first stage (the hierarchical clustering stage), the number of clusters was selected, the mean trajectories of clusters were defined, which were further used as seeds to start the second stage (the k-means clustering stage). However, this clustering method often resulted in long trajectories being highly separated, even though they originated from the same geographical region, since the Euclidean

distances between endpoints within longer trajectories were very large. In contrast, many short trajectories representing slow-moving air masses were grouped together even though they came from very heterogeneous regions (Borge et al., 2007).

To achieve better representation of slow-moving air masses, after implementing the two-stage clustering procedure for the first time, trajectories within shorter clusters (or cluster) were grouped together as a new sample and re-clustered by the two-stage clustering procedure again to generate new short-trajectory clusters.

A vital problem in applying the clustering method is selection of a reasonable number of clusters the hierarchical clustering stage. A classic selection method involves analysis of the percentage change in root mean-square deviation (RMSD) with change in the number of clusters (Dorling et al., 1992). However, the results produced by this method were not satisfactory. RMSD results did not represent well the airflow classifications because too many clusters were similar or even overlapped. We obtained nine clusters in total, six of which generally came from the northwest. What was more, the RMSD failed to provide a clear description of the slow-moving air masses that had been found to cause high concentrations of PM_{10} in Beijing (An et al., 2006; Chen et al., 2008).

Therefore, we used the "jump points" of the fusion coefficients instead. Fusion coefficients provide an index of the relative distance of trajectories being merged at each stage of the hierarchical clustering stage (Aldenderfer and Blashfield, 1984). We calculated the fusion coefficients of each cluster number from one to ten. These fusion coefficients were plotted against the associated number of clusters. A jump point of a fusion coefficient is the point at which the fusion coefficient increases greatly when the number of clusters decreases by one. The jump point indicates that two relatively dissimilar clusters have been merged, and thus the number of clusters prior to the merger is the most probable cluster solution.

2.4. TSA method

Twelve 30° sectors were used to evaluate the influence of air mass direction on PM_{10} concentrations. Sector 1 was from due north and 30° east of north; sectors 2–12 were numbered in a clockwise direction with increment of 30° (see Fig. 3). The location of the trajectory during the first 6 h was excluded since the sectors could be not well-defined close to the origin, and a small amount of curvature in a trajectory can lead to spurious results (Bari et al., 2003). Equations (1)–(3) were used to calculate the mean concentration from sector j (C_j) and the relative contribution from sector j ($\%C_j$),

$$C_j = \frac{\sum_{i=1}^{N} C_i f_{ij}}{N_j}, \tag{1}$$

$$N_j = \sum_{i=1}^{N} f_{ij}, \tag{2}$$

$$\%C_j = \frac{C_j N_j}{\sum_{j=1}^{12} C_j N_j} 100, \tag{3}$$

where N is the total number of trajectories, C_i is the concentration of PM_{10} within the ith trajectory, f_{ij} is the time passed through sector j for the ith trajectory, and N_j is the total time during which trajectories passed through sector j.

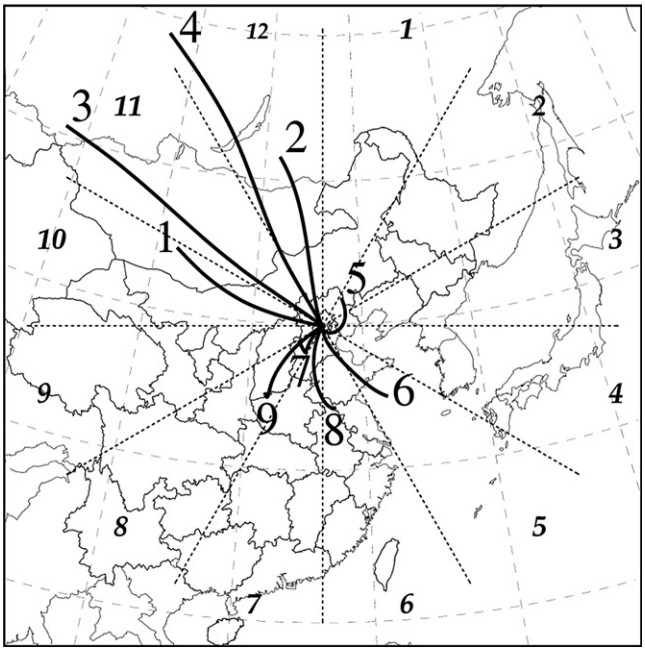

Fig. 3. Mean 72-h backward trajectories of the nine clusters. Dashed lines denoted 12 sectors (numbered in italics).

2.5. PSCF method

The PSCF value can be understood as a conditional probability that describes the spatial distribution of probable source locations. The domain for PSCF computation stretched 76° in latitude and 76° in longitude with the center of Beijing (39°54′27″N, 116°23′17″E), containing 23,104 grid cells of 0.5° × 0.5°.

The staying time of all trajectories in a single grid cell is n_{ij}, and m_{ij} is the staying time in the same cell that correspond to the trajectories that arrived at a receptor site with pollutant concentrations higher than a pre-specified criterion value (70th percentile of PM_{10} concentrations was used in this study). The PSCF value for the ij^{th} cell is then defined as

$$\mathrm{PSCF}_{ij} = \frac{m_{ij}}{n_{ij}}. \tag{4}$$

To remove the large uncertainty caused when a grid cell has small staying time and large PSCF values, usually a weight function $W(n_{ij})$ is multiplied into the PSCF value to better reflect the uncertainty in the values for these cells (Polissar et al., 2001a,b). In our study the $W(n_{ij})$ was:

$$W(n_{ij}) = \begin{cases} 1.00 (80 < n_{ij}) \\ 0.70 (25 < n_{ij} \le 80) \\ 0.42 (15 < n_{ij} \le 25) \\ 0.17 (n_{ij} \le 15) \end{cases} \tag{5}$$

The $W(n_{ij})$ values were based on former researches (Polissar et al., 2001a,b; Han et al., 2005). The classification of n_{ij} was obtained empirically by running the PSCF Fortran program many times. Being similar to the studies of Polissar et al. (2001a,b), classifications leaded to high unrealistic attribution of source areas were excluded. For example, the north and east of Beijing where no high PM_{10} sources located was not expected to have high PSCF value. Finally, regions with high PSCF values were regarded as the potential sources.

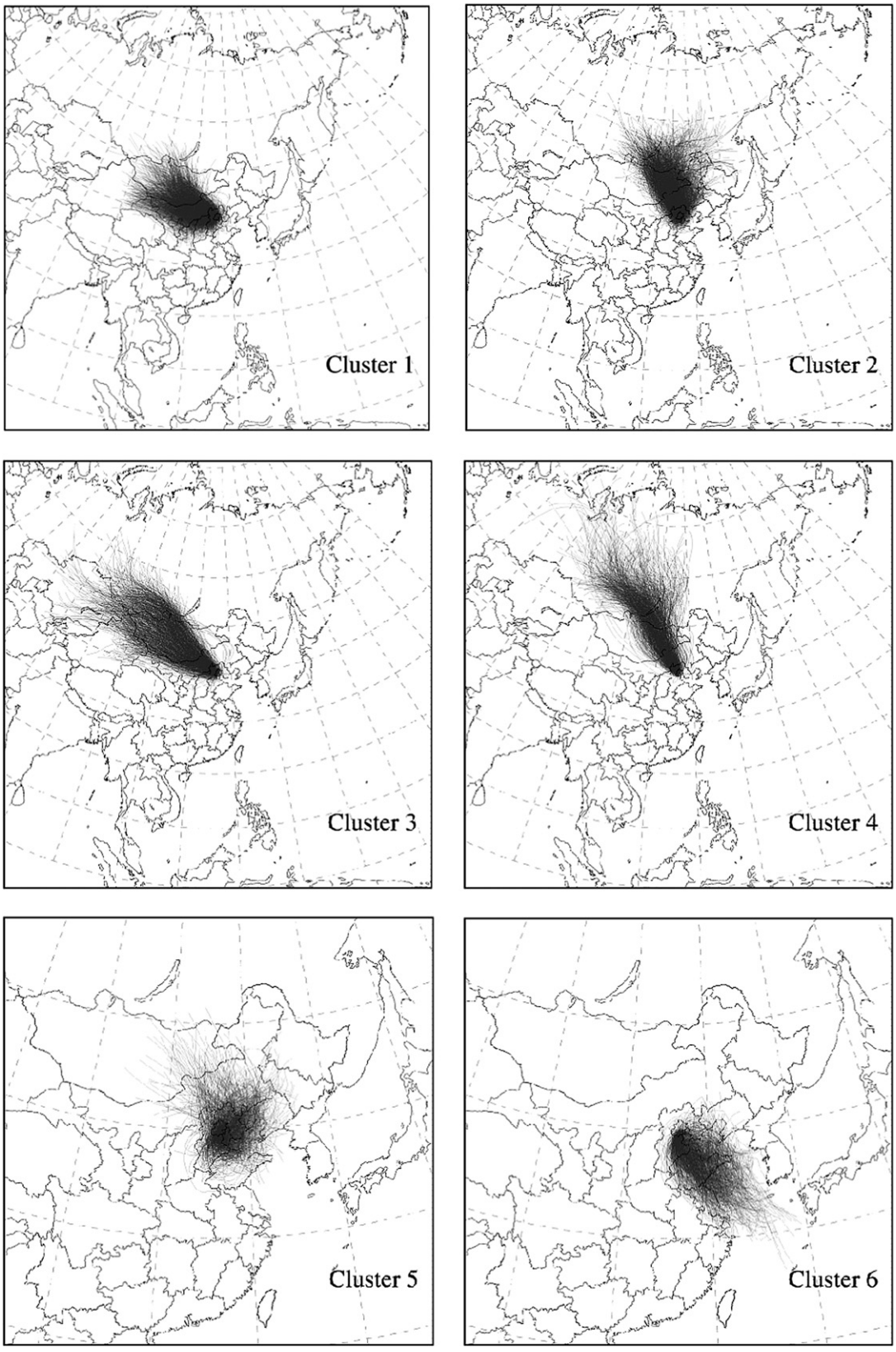

Fig. 4. Seventy-two-hour backward trajectories within the nine clusters.

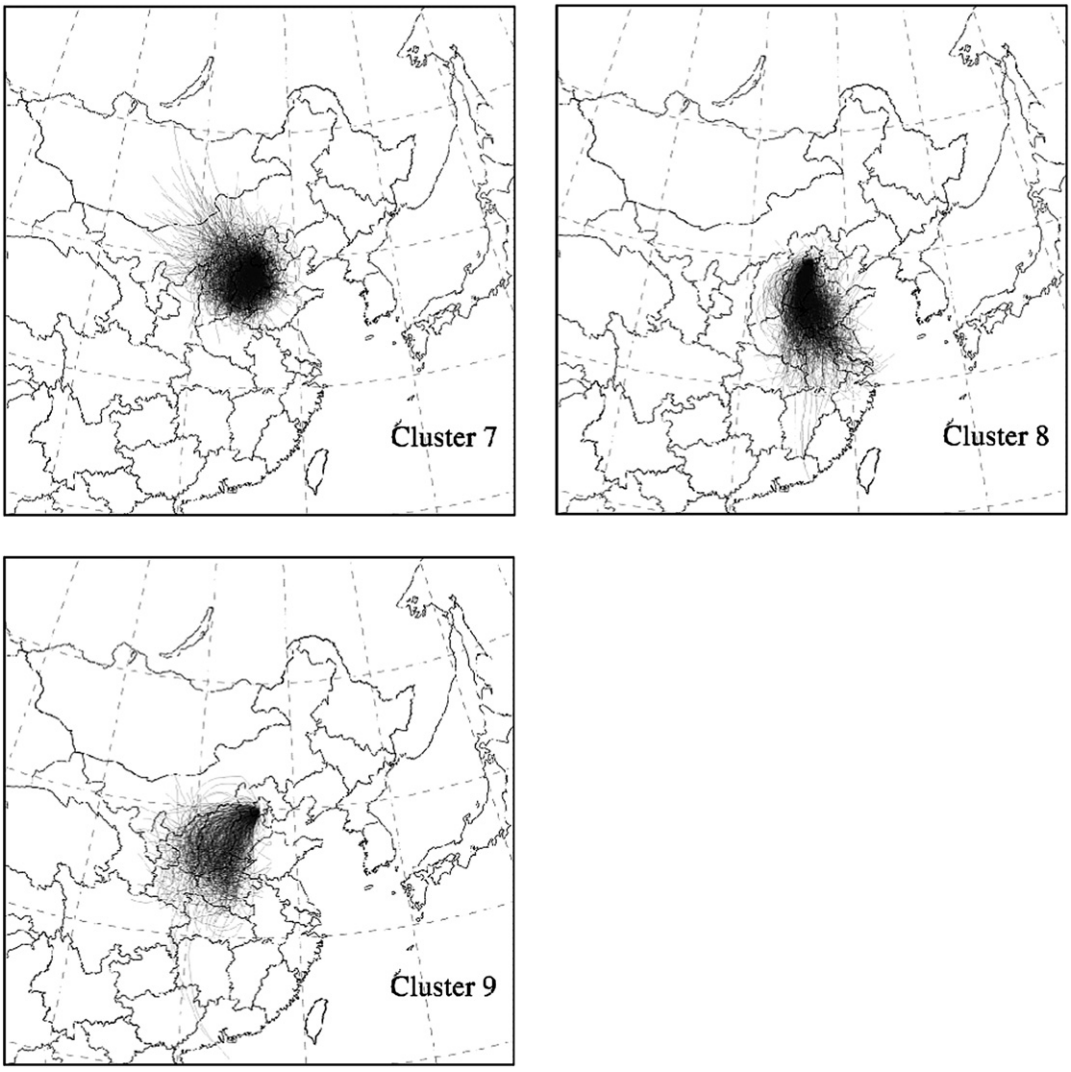

Fig. 4. (*continued*).

3. Results and discussion

3.1. Clustering results

In the average-linkage clustering stage, no obvious jump point could be determined. We tried using four–ten clusters. After a visual inspection, we chose five as the number of clusters because this gave the best representation of airflow classifications. Among those five clusters, four relatively long clusters were retained; trajectories within the shorter cluster were re-clustered into five shorter clusters based on an obvious jump point. Finally we got nine clusters. The number of trajectories in nine clusters was 1912, 1978, 1274, 1029, 878, 930, 975, 815, and 413, respectively. Fig. 3 illustrates the mean trajectories of each cluster and Fig. 4 shows the trajectories within each cluster.

Fig. 5 presents the monthly frequencies of the nine clusters. We tried to link the frequency of each cluster with the monsoon climate in North China. In winter, North China is located southeast of the Mongolian high and thus a northerly flow prevails (clusters #1, #3, and #4). During the spring, the Mongolian high decreases and moves back to the northwest, and the winter monsoon transitions to the summer monsoon. In summer, the weather is controlled by the India low and the Pacific subtropical high. North China is located in a flat trough, and thus southerly flow is more frequent at this time (clusters #5, #6, and #8). In autumn, the summer monsoon transitions to the winter monsoon. Trajectories within cluster #7 did not show a clear direction (Fig. 4), possibly reflecting the seasonal conversion of the monsoon (Gu, 1991).

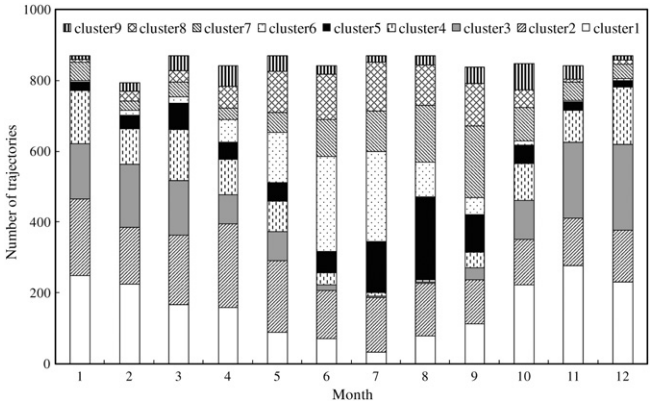

Fig. 5. Frequency of occurrences for the nine clusters in each month during the study period.

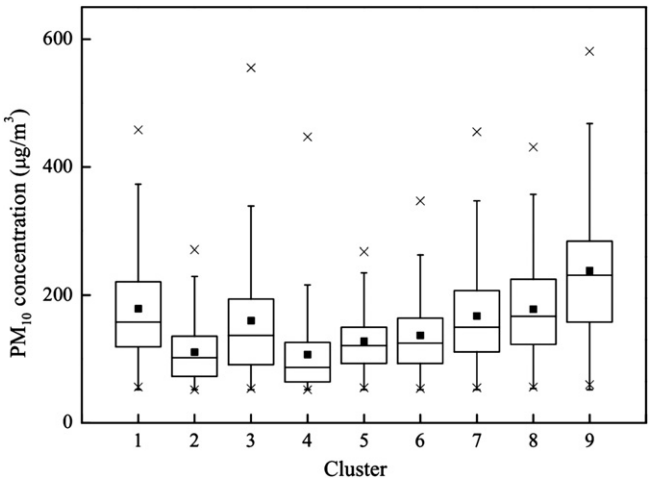

Fig. 6. PM_{10} concentrations within the nine clusters. A solid square denotes the mean. The horizontal line across the box is the median, the lower and upper hinges represent the 25th and 75th percentiles, respectively, while the lower and upper cross represent the 1th and 99th percentiles, respectively.

Trajectories within different clusters of airflow had distinct effects on the PM_{10} concentrations (Fig. 6). Mean PM_{10} concentration was 180.1, 109.3, 160.8, 106.8, 126.8, 130.7, 165.3, 176.0 and 234.0 and 149.7 μg m^{-3} for clusters #1–#9, respectively. The highest PM_{10} concentration was found in cluster #9, while the lowest PM_{10} concentrations were found in clusters #2 and #4. A Kruskal–Wallis test (Brankov et al., 1998) was applied to test the significance of inter-cluster variation in PM_{10} concentration. The results showed a statistically significant ($p < 0.05$) difference in PM_{10} concentrations among clusters. A Dunn test (Bonferroni test) (Brankov et al., 1998) was then used to determine which clusters differed from the others. Only the PM_{10} concentrations within cluster pairs #2 and #4, #1 and #8, #3 and #7, and #5 and #6 had no significant differences ($p > 0.05$), while PM_{10} concentrations within any of the remaining pairs of clusters were significantly different. Given that trajectories in clusters #2 and #4 traveled in a similar direction, we merged them as the northern pathway (see Section 3.2.7).

3.2. Transport pathways and potential sources

Here we discuss PM_{10} transport pathways in Beijing based on the clustering, TSA, and PSCF results. High PM_{10} concentrations in the TSA sectors would imply high polluted pathways. Along such pathways, the high emissions could probably located, which were indicated by high PSCF values.

3.2.1. The southwest pathway (cluster #9)

The southwest pathway was based on cluster #9 (Figs. 3 and 4). Trajectories in this pathway mainly moved in a southwesterly direction and frequently occurred in April and October (Fig. 5), months characterized by conversions between the summer and winter monsoons (Zhou, 1989). The high frequency of this pathway in April and October may have contributed to high PM_{10} concentrations in Beijing in spring and autumn (Fig. 2). The highest PM_{10} concentrations (Fig. 6) along the southwest pathway were probably associated with emissions from Shanxi and the south and west of Hebei (Fig. 7). Shanxi, the center of China's energy, metallurgy, and coal chemical industries, has had serious air pollution problems in recent years, coinciding with the rapid development of these highly polluting industries. In 2004, air quality in 28 Chinese cities was below the National Grade III standard, and five of these cities were located in Shanxi. Among them, Linfen and Yangquan, the two most polluted cities, were located along the southwest pathway (Niu and Ren, 2006). Anthropogenic emissions in the west and south of Hebei were also considerable (Fig. 7) (including high vehicular emission, Cai and Xie, 2007), which was supported by a large amount of urban land in that region (Fig. 8).

Moreover, calm winds often prevailed at the eastern foot of Mount. Taihang (e.g., Weixian, Fuping, Shijiazhuang, and Shexian; Fig. 9, Table 1) and over the southern Hebei Plain (e.g., Baoding, Xingtai, and Handan; Fig. 9, Table 1). Thus, the pollutants in this calm zone were not likely to diffuse, and serious air-quality

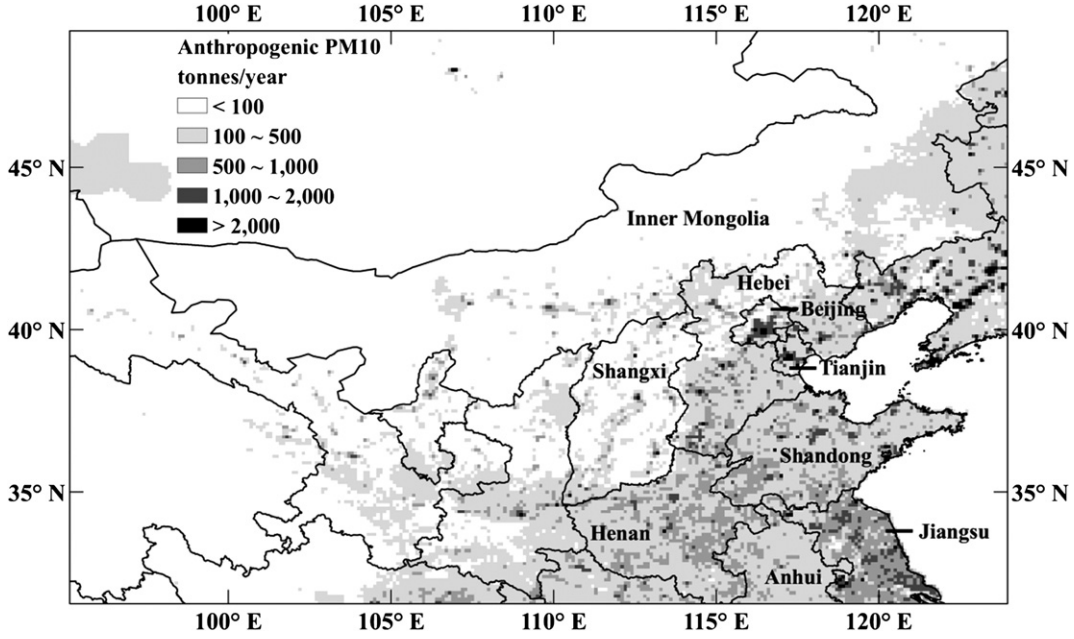

Fig. 7. Distribution of anthropogenic emissions of PM_{10} in the north of China. Emission data was from Streets et al. (2003), with a 6-min resolution updated from the TRACE-P emissions inventory.

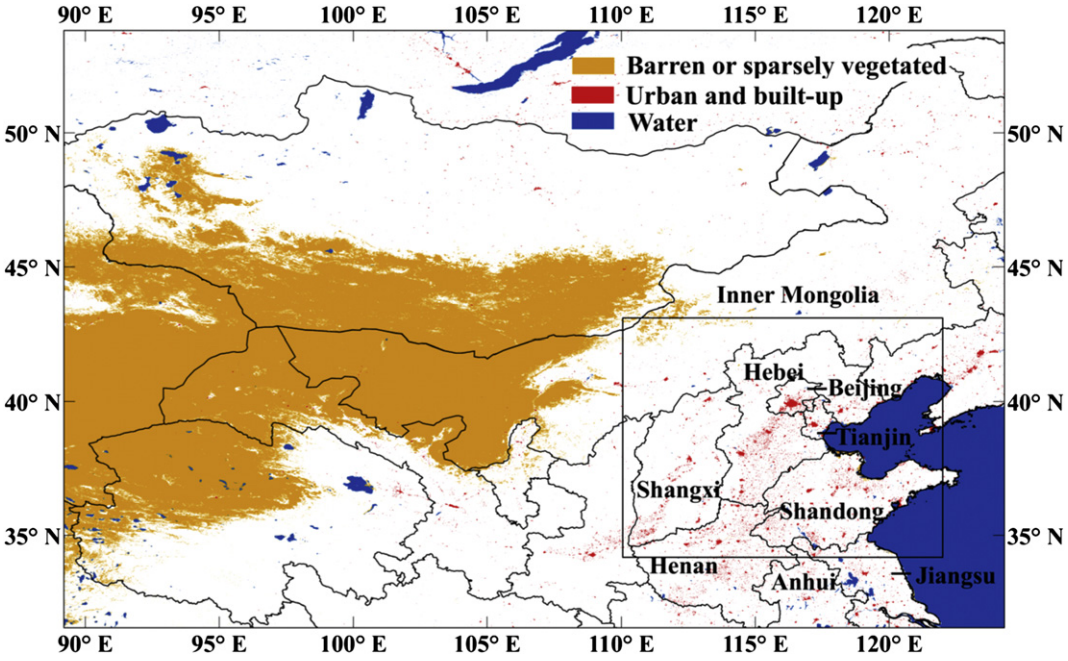

Fig. 8. Barren or sparsely vegetated land and urban and built-up land in North China. Data from The Moderate Resolution Imaging Spectroradiometer (MODIS) MCD12Q1 product (year 2007), available from https://lpdaac.usgs.gov/lpdaac/products/modis_products_table/land_cover/yearly_l3_global_500_m/mcd12q1.

problems probably arise because of the accumulation of air pollutants. Hence, the highest concentration of PM_{10} along the southwest pathway was probably due to a combination of high emissions and the calm zone.

Mean PM_{10} concentrations for sectors 7–9 were highest (Fig. 10a), which was in good agreement with the most polluted southwest pathway. The southwest pathway traveled over the Loess Plateau (potential source S1) and the west and south of Hebei (potential source S2) (Fig. 11).

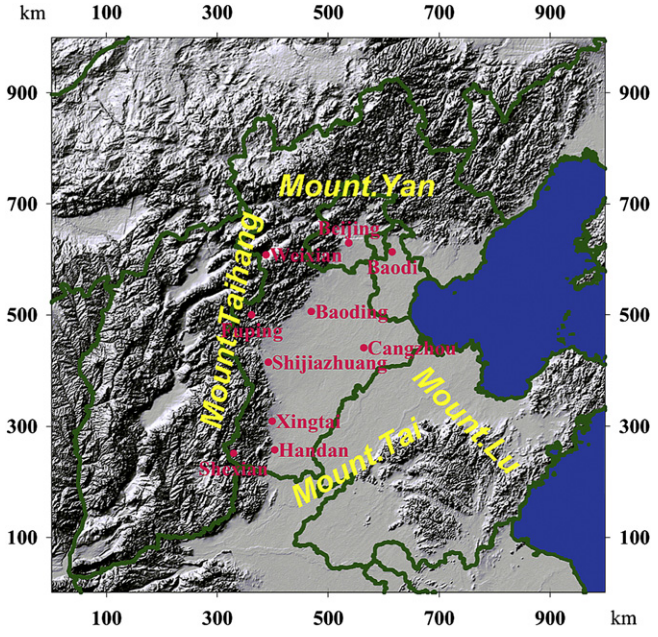

Fig. 9. Topography of regions near Beijing (1000 km × 1000 km). The approximate and limit of Fig. 9 is the inner rectangle in Fig. 8.

3.2.2. The south pathway (cluster #8): the summer monsoon and topographic effects

The south pathway was based on cluster #8 (Figs. 3 and 4) and was frequently occurred from May to September (Fig. 5), possibly in association with the summer monsoon (Gu, 1991) and topographic effects. Due to friction (Fig. 9), warm and moist air masses from the south curve cyclonically on the eastern side of Mount. Taihang and anti-cyclonically on the western sides of Mount. Tai and Mount. Lu, ultimately resulting in a prevailing southerly wind on the Southern Hebei Plain (Gu, 1991). High PM_{10} concentrations along this pathway were probably related to emissions from the east of Henan, the north of Jiangsu, the middle and west of Shandong, and the west and south of Hebei (Fig. 7) (including high vehicular emission, Cai and Xie, 2007), which was supported by considerable extent of urban land in those regions (Fig. 8). In addition, the calm wind zone along the pathway may have increased concentrations of PM_{10} even further.

High mean PM_{10} concentrations were found in sectors 6 and 7 (Fig. 10a), reflecting the highly polluted nature of the southern pathway. The relative contribution from sector 7 was high, indicating that a high contribution arrived from the south. The south pathway passed over potential source S2 and the north of Anhui, Henan, and Jiangsu and west of Shandong (potential source S3) (Fig. 11).

3.2.3. The northwest pathway (clusters #1 and #3): the Mongolian high and the Mongolian cyclone

The northwest pathway was based on clusters #1 and #3 (Figs. 3 and 4). Cluster #1 frequently occurred in autumn and winter, followed by spring and then summer (Fig. 5). The west–northwesterly flow that characterizes clusters #1 and #3 may have been associated with the Mongolian high and Mongolian cyclones. In winter, when the Mongolian high is active, the East Asian continent is under the control of a strong northwesterly flow. In spring and autumn, cold and warm airs appear frequently, and activity of the Mongolian cyclone is strong (Wang, 1990). The trajectories in cluster #3 were longer than those in cluster #1 (Figs. 3 and 4),

Table 1
Frequencies (%) of the two most frequent wind directions in every month and the whole year on the east of Mount. Taihang.[a]

	1	2	3	4	5	6	7	8	9	10	11	12	Whole year	Data period
Weixian	C 48 SW 7	C 40 N/SW 6	C 32 N 8	C 24 SW 11	C 24 SW 10	C 28 SE/SW 8	C 38 SSE 7	C 42 SE/SW 7	C 40 SW 7	C 41 SW 7	C 40 SW 8	C 44 W/SW 6	C 37 SW 8	1960–1974
Fupin	C 53 SE 11	C 41 SE 12	C 38 SE 11	C 28 NW 14	C 26 SE16	C 26 SE16	C 31 SE16	C 38 SE17	C 38 NW 13	C 45 NW 11	C 46 NW 12	C 40 NW 14	C 38 SE/NW 8	1960–1961 1972–1974
Baoding	C 20 N 11	C 16 SW 13	C 14 SW 11	SW 13 N 12	SW 16 SSW 12	C 14 SW 12	C 23 SW 12	C 26 N 13	C 24 SW 13	C 21 SW 14	C 18 SW 14	C 22 SW 12	C 18 SW 12	1960–1974
Shijiazhuang	C 34 N 10	C 32 N 10	C 28 N 10	C 28 SE 12	C 29 SE 12	C 33 SE 12	C 41 SE 10	C 48 N/SE 8	C 44 SE 8	C 42 N 9	C 37 NW 8	C 37 N/NW 7	C 36 SE 9	1960–1974
Xingtai	C 19 N 15	C 16 N 15	S 19 N 16	S 25 N 13	S 28 N 12	S 23 N 13	S 17 N 16	C 22 N 16	C 24 S 16	C 24 S 16	C 20 N 15	C 21 N 13	C/S 17 N 17	1960–1974
Shexian	C 31 NE 15	C 28 NE 22	C 26 NE 16	C 29 NE 13	C 34 S 7	C 29 NE/S 9	C 38 NE10	C 42 NE 14	C 46 NE 12	C 39 NE 13	C 32 NE 11	C 31 NE 11	C 34 NE 12	1962–1971
Handan	C 20 CN 14	C 19 N 14	S 16 N 13	S 17 N 13	S 21 SSW 15	S 19 C/SSW 12	C 19 S 14	C 24 N 12	C 22 S 14	C 25 S 15	C 18 N 14	C 18 N 13	C 17 S 14	1960–1966 1971–1974
Cangzhou	C 12 SSW/SW 9	SSW 10 C/SW 9	SSW 14 SW 10	SSW 16 S 10	SSW 19 SW 12	SSW 15 E 10	C/SSW 11 S 9	C 16 NE/E/S/SSW 8	C/SSW 13 S/SW 9	SSW 15 C/SW 10	SSW 13 C 12	SSW 13 C 12	SSW 13 C/SW 9	1960–1974

[a] Date from Headquarters of Hebei Military region (1978). 'C' represents for calm winds, and '/' means that the two have equal frequency.

which may have resulted from a deeper Mongolian high in winter. The high frequency of this pathway in spring may have contributed to the high spring PM_{10} concentrations in Beijing (Fig. 2).

Low emissions (Fig. 7) were found in northwest Beijing where there is little urban land (Fig. 8). The northwest pathway may link to strong winds that dislodge and transport dust and sand along the pathway (Fig. 8). This pathway was consistent with a pathway of dust and sand identified by Wang et al. (2004). The PM_{10} concentration of cluster #1 was higher than that of cluster #3 (Fig. 6), which may be the result of cluster #1 having a higher frequency of occurrence in spring. The Mongolian cyclone assisted by a cold front is the major weather system leading to dust events in Beijing (Yin et al., 2007), and both of these systems are more frequent in spring.

Sectors 10 and 11 had the highest relative contributions (Fig. 10a), which means that the highest contributions came from the northwest. The northwest pathway passed over potential source S1, the south of Mongolia, and the west of Inner Mongolia (potential source S4) (Fig. 11).

3.2.4. The V-shaped southwest pathway (cluster #7)

The V-shaped southwest pathway was based on cluster #7 (Figs. 3 and 4). This pathway represents relatively short and no-special-directional trajectories from Hebei and Shanxi (Fig. 4). Airflows along this pathway gathered at Mount. Taihang and moved from the southwest, with the highest frequency of occurrence in September (Fig. 5). Air masses along this pathway may have been related to the

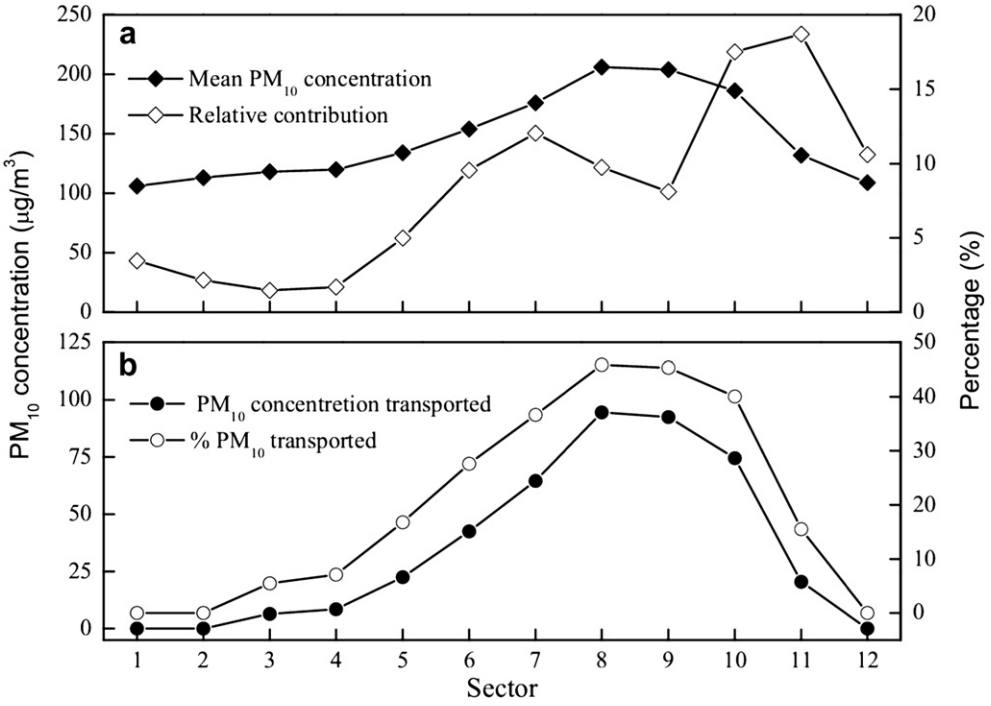

Fig. 10. (a) Angular concentration and contribution profile for PM_{10} based on the TSA method; (b) Transported PM_{10} concentration and contribution of each sector.

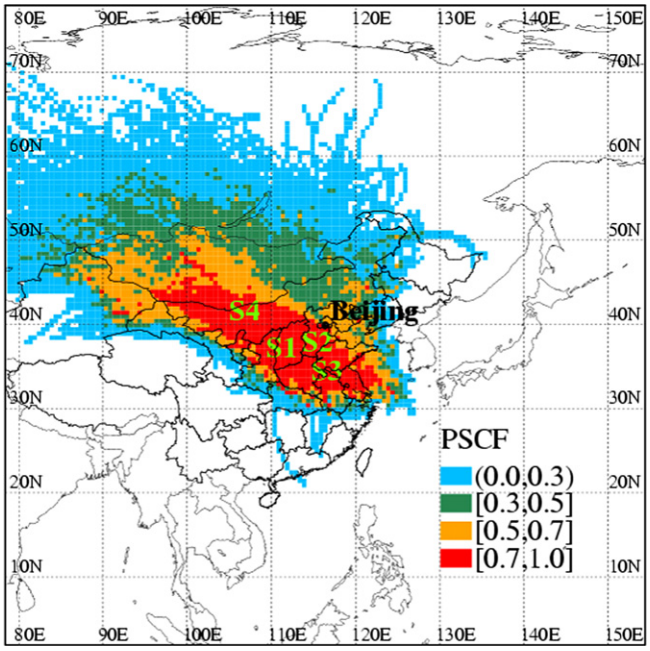

Fig. 11. PSCF map for PM_{10} and potential sources of PM_{10} in Beijing. S1: Loess Plateau; S2: the west and south of Hebei; S3: the north of Anhui, Henan, and Jiangsu and west of Shandong; and S4: the south of Mongolia, and the west of Inner Mongolia.

conversion of the summer monsoon to the winter monsoon in early autumn (Zhou, 1989). This V-shaped pathway agreed with the local frequency of wind directions. In Fuping and Baoding, calm wind (Fig. 9, Table 1) was the most frequent wind in September, followed by wind from the northwest and southwest directions, respectively (Table 1).

The high frequency of this pathway in September may have contributed to high autumn PM_{10} concentrations in Beijing (Fig. 2). High concentrations of PM_{10} along this pathway could have originated from emissions in eastern Shanxi and western and southern Hebei. The calm wind zone on the pathway may also have contributed to the increased PM_{10} concentration. This slow-moving southwest pathway agrees with that found in a case study based on model stimulations (An et al., 2006), which identified high concentrations of PM_{10} transported from the southwest area of Beijing to the northeast by west and southwest winds under weak wind situations. The pathway also agrees with conceptual descriptions of pathways reported by Chen et al. (2008). Mean PM_{10} concentrations were the highest for sectors 7–9 (Fig. 10a), which correspond to the highly polluted V-shaped southwest pathway that passes over potential sources S1 and S2 (Fig. 11).

3.2.5. The southeast pathway (cluster #6): the summer monsoon

The southeast pathway, based on cluster #6 (Figs. 3 and 4), frequently occurred in June and July (Fig. 5) and may have been affected by the summer monsoon (Wang, 2005). The high frequency of this relatively clean pathway in June and July may have contributed to low PM_{10} concentrations in Beijing during summer (Fig. 2). The southeast pathway was probably affected by emissions from Shandong, Tianjin, and the north of Jiangsu. Although emissions were considerable in these regions (Fig. 7), plentiful precipitation in summer may have offset the increasing trend of PM_{10} concentrations by wet deposition. Summer precipitation accounted for about 75% of the annual precipitation in Beijing (Beijing Meteorology Bureau, 1987). In addition, air masses traveling with this pathway may have avoided the calm wind zone in the west and south of Hebei. For example, the frequency of calm wind in Cangzhou (Fig. 9), which is located southeast of Hebei, was not very high compared to that in cities lying west and south of Hebei (Table 1). Average PM_{10} concentrations for sectors 4 and 5 were relatively low (Fig. 10a), which is consistent with the less polluted southeast pathway. Furthermore, PSCF values were low for regions located along this pathway (Fig. 11).

3.2.6. The curved east pathway (cluster #5): the summer monsoon

The east pathway was based on cluster #5 (Figs. 3 and 4) and occurred frequently in August (Fig. 5). The mean backward trajectory of this pathway was curved, showing a northeast direction. Easterly flow may be associated with the summer monsoon, while northerly flow may result from northwesterly weather systems that occur throughout the year. The easterly flow in July and August (peak occurrence months for cluster #5) matched local records of wind frequency in the north of Tianjin (Headquarters of the Tianjin Military Region, 1979), which showed that east wind was the most frequent in July and August for Baodi (Fig. 9). The high frequency of this relatively clean pathway in July and August may have contributed to low summer PM_{10} concentrations in Beijing (Fig. 2). This pathway was probably affected by emissions from Tianjin and Hebei. The frequency of occurrence of this pathway peaked in August, which corresponds to peak precipitation in Beijing. Precipitation during July and August in Beijing accounts for about 65% of the annual value (Beijing Meteorology Bureau, 1987). Intensive wet deposition may lead to relatively low PM_{10} concentrations. Both the mean PM_{10} concentrations and relative contributions to PM_{10} in Beijing were low for sectors 2–4 (Fig. 10a). Low PSCF values were also found for regions along this pathway (Fig. 11).

3.2.7. The northern pathway (clusters #2 and #4): the Mongolian high, the Mongolian cyclone, and the Northeast China low

The northern pathway, including clusters #2 and #4 (Figs. 3 and 4), was the cleanest pathway (Fig. 6). Airflows included in cluster #2 mainly traveled from the north, with the highest frequency of occurrence in spring and a nearly consistent frequency of occurrence in winter, autumn, and summer (Fig. 5). Air masses in cluster #2 may have resulted from the Mongolian cyclone or the Northeast China low. The Mongolian cyclone occurs throughout the year, with a higher frequency of occurrence in spring, and usually moves eastward and then forms the Northeast China low (Liu, 1986). Air masses in cluster #4, which had the highest frequency of occurrence in winter, followed by spring and then summer (Fig. 5), mainly passed along a northwest direction. These air masses may be linked to the Mongolian high. Few anthropogenic PM_{10} (Fig. 7) sources and little barren land (Fig. 8) were located on this pathway. Also, PM_{10} in Beijing was likely to diffuse due to the strong winds associated with this pathway. The lowest PM_{10} concentrations were associated with sectors 1 and 12 (Fig. 10a). Relatively low PSCF values were also found for regions located along this pathway (Fig. 11).

3.3. Background versus long distance transportation of PM_{10}

Here we roughly estimate the background and long distance transported PM_{10} in Beijing based on the methods of Bari et al. (2003). The clustering (Fig. 6) and TSA (Fig. 10a) results indicated that trajectories from the south and west were associated with high PM_{10} concentrations, while trajectories from the east and north were associated with relatively low PM_{10} concentrations. This result was supported by PM_{10} concentrations at two rural sites and two suburban sites (Fig. 1a, Table 2). The PM_{10} concentrations in Yanqing and Miyun were lower than those in Beijing, Fangshan, and Tongzhou. So we estimated the background concentrations based

Table 2
Basic statistics (in μg m^{-3}) of PM_{10} concentrations in rural, suburban and urban cites.

Site	Mean	Percentile 25	Median	Percentile 75	Std deviation
Yanqing	132.0	80.0	114.0	162.0	72.5
Miyun	138.7	82.0	122.0	168.0	77.6
Tongzhou	155.3	96.0	134.0	188.0	84.9
Fangshan	175.9	110.0	150.0	218.0	93.4
Beijing[a]	150.4	91.0	134.0	185.0	84.1

[a] Average values from the eight urban sites (Fig. 1b).

on the trajectories reaching Beijing from sectors 1, 2, 3, and 12 (east and north). The mean PM_{10} concentration from these sectors, defined as the "local background," was 111.5 μg m^{-3}. Fig. 10b shows the concentrations and contributions of transported components after subtracting the background PM_{10}. Sectors 7–10 contributed the most PM_{10}, with concentrations of 64.5, 94.5, 92.5, and 74.5 μg m^{-3}, contributing 36.6%, 45.9%, 45.1%, and 40.1%, respectively, to the mean concentration of PM_{10} in each sector. By combining the transported concentrations and the percent frequency of air masses from various sectors, we determined that the contribution of long distance transported PM_{10} in Beijing was about 39.3 μg m^{-3}, which would account for about 26.0% of the PM_{10} concentration in Beijing.

4. Conclusions

In this study, trajectory clustering and PSCF methods were used to investigate the transport pathways and potential sources of PM_{10} in Beijing based on 2003–2009 data. Nine clusters of backward trajectories were generated, including four long clusters possibly caused by the winter monsoon and five short clusters possibly resulting from the summer monsoon and topographic effects.

Four transport pathways of high concentrations of PM_{10} were identified. The northwest pathway may have been associated with dust and sand in northwest Beijing and anthropogenic emissions from Shanxi. The south pathway and the V-shaped southwest pathway were linked to anthropogenic emissions from the south of Beijing. The highest PM_{10} concentration was found along the southwest pathway, which may have been affected by anthropogenic emissions from the Loess Plateau and the west and south of Hebei. Moreover, the frequent occurrence of calm winds in the south of Beijing could have contributed to the accumulation of air pollutants.

The southeast pathway and the curved eastern pathway were linked to relatively low concentrations of PM_{10} in Beijing, possibly due to wet deposition caused by intensive precipitation in summer. The lowest PM_{10} concentration was found for the northern pathway, and may have resulted from low emissions and strong winds that aided diffusion.

Both natural sources of dust and sand in southern Mongolia and western Inner Mongolia and anthropogenic sources in Shanxi and Hebei had significant impacts on the high concentrations of PM_{10} in Beijing. Reducing anthropogenic PM_{10} emissions from the coal industry, transportation, and construction in Shanxi and Hebei could be an effective way to control PM_{10} pollution in Beijing.

It was also found that the contribution of PM_{10} from long transported was about 39.3 μg m^{-3} accounting for about 26.0% of the PM_{10} concentrations in urban Beijing.

Acknowledgments

This study was funded by Chinese National Science Foundation (40975088), the National Key Basic Research and Development Program of China (2008AA06A415), the Public Welfare Projects for Environmental Protection (200809018, 200709001), and the New-Century Training Program Foundation for Talents from the Ministry of Education of China. The authors thank Steven Q. Andrews at University of California, Los Angeles for providing API data he collected from BJEPB. The authors would also like to thank two anonymous reviewers for their comments in improving this paper.

References

Aldenderfer, M.S., Blashfield, R.K., 1984. Cluster Analysis. Sage, Newbury Park (CA).
An, X., Zhu, T., Wang, Z., Li, C., Wang, Y., 2006. A modeling analysis of a heavy air pollution episode occurred in Beijing. Atmos. Chem. Phys. Discuss. 6, 8215–8240.
Ashbaugh, L.L., Malm, W.C., Sadeh, W.Z., 1985. A residence time probability analysis of sulfur concentrations at Grand Canyon National Park. Atmos. Environ. 19 (8), 1263–1270.
Bari, A., Dutkiewicz, V.A., Judd, C.D., Wilson, L.R., Luttinger, D., Husain, L., 2003. Regional sources of particulate sulfate, SO_2, $PM_{2.5}$, HCl, and HNO_3, in New York, NY. Atmos. Environ. 37 (20), 2837–2844.
Beijing Environmental Protection Bureau (BJEPB), 2003–2009. Daily API Report. http://www.bjepb.gov.cn/ (in Chinese).
Beijing Environmental Protection Bureau annual report, 2000–2008. Bulletin of Environment State in Beijing. http://www.bjepb.gov.cn/bjhb/publish/portal0/tab375/ (in Chinese).
Beijing Meteorology Bureau, 1987. Climatography of Beijing. Beijing Press, Beijing (in Chinese).
Borge, R., Lumbrera, J., Vardoulakis, S., Kassomenos, P., Rodríguez, E., 2007. Analysis of long-range transport influence on urban PM_{10} using two-stage atmospheric trajectory clusters. Atmos. Environ. 41 (21), 4434–4450.
Brankov, E., Rao, S.T., Porter, P.S., 1998. A trajectory-clustering-correlation methodology for examining the long-range transport of air pollutants. Atmos. Environ. 32 (9), 1525–1534.
Cai, H., Xie, S.D., 2007. Estimation of vehicular emission inventories in China from 1980 to 2005. Atmos. Environ. 41 (39), 8963–8979.
Cape, J.N., Methven, J., Hudson, L.E., 2000. The use of trajectory cluster analysis to interpret trace gas measurements at Mace Head, Ireland. Atmos. Environ. 34 (22), 3651–3663.
Chan, C.K., Yao, X., 2008. Air pollution in mega cities in China. Atmos. Environ. 42 (1), 1–42.
Chen, Z.H., Cheng, S.Y., Su, F.Q., Gao, Q.X., 2008. Analysis of synoptic patterns and transports during regional atmospheric pollution process in north China. Res. Environ. Sci. 21 (1), 17–21 (in Chinese).
Davis, R.E., 1991. A synoptic climatological analysis of winter visibility trends in the mid-eastern United States. Atmos. Environ. B Urban Atmos. 25 (2), 165–175.
Dorling, S.R., Davies, T.D., Pierce, C.E., 1992. Cluster analysis: a technique for estimating the synoptic meteorological controls on air and precipitation chemistry—method and applications. Atmos. Environ. 26A (14), 2575–2581.
Eder, B.K., Davis, J.M., Bloomfield, P., 1994. An automated classification scheme designed to better elucidate the dependence of ozone on meteorology. J. Appl. Meteorol. 33 (10), 1182–1199.
Gu, T.M., 1991. Climate in North China Plain. China Meteorological Press, Beijing (in Chinese).
Han, Y.-J., Holsen, T.M., Hopke, P.K., Yi, S.-M., 2005. Comparison between back-trajectory based modeling and Lagrangian backward dispersion modeling for locating sources of reactive gaseous mercury. Environ. Sci. Technol. 39 (6), 1715–1723.
Headquarters of Hebei Military Region, 1978. Military Climate in Hebei (in Chinese).
Headquarters of Tianjin Military Region, 1979. Military Climate in Tianjin (in Chinese).
Liu, Z.L., 1986. Synoptic Meteorology. China Meteorological Press, Beijing (in Chinese).
Moody, J.L., Galloway, J.N., 1988. Quantifying the relationship between atmospheric transport and the chemical composition of precipitation on Bermuda. Tellus Ser. B Chem. Phys. Meteorol. 40B (5), 463–479.
Niu, R.L., Ren, Z.H., 2006. Study on Effects of Inter-regional Air Pollution: a Case Analysis of the Impact of Air Pollution from Shanxi on Beijing. Science Press, Beijing (in Chinese).
Oanh, N.T.K., Chutimon, P., Ekbordin, W., Supat, W., 2005. Meteorological pattern classification and application for forecasting air pollution episode potential in a mountain-valley area. Atmos. Environ. 39 (7), 1211–1225.
Ostro, B., Broadwin, R., Green, S., Feng, W.Y., Lipsett, M., 2006. Fine particulate air pollution and mortality in nine California counties: results from CALFINE. Environ. Health Perspect. 114 (1), 29–33.
Parekh, P.P., Husain, L., 1982. Ambient concentrations and windflow patterns at Whiteface mountains. Geophys. Res. Lett. 9 (1), 79–82.
Parrish, D.D., Kuster, W.C., Shao, M., Yokouchi, Y., Kondo, Y., Goldan, P.D., de Gouw, J.A., Koike, M., Shirai, T., 2009. Comparison of air pollutant emissions among mega-cities. Atmos. Environ. 43 (40), 6435–6441.
Polissar, A.V., Hopke, P.K., Harris, J.M., 2001a. Source regions for atmospheric aerosol measured at Barrow, Alaska. Environ. Sci. Technol. 35 (21), 4214–4226.
Polissar, A.V., Hopke, P.K., Poirot, R.L., 2001b. Atmospheric aerosol over Vermont: chemical composition and sources. Environ. Sci. Technol. 35 (23), 4604–4621.

Qureshi, S., Dutkiewicz, V.A., Khan, A.R., Swami, K., Yang, K.X., Husain, L., Schwab, J.J., Demerjian, K.L., 2006. Elemental composition of $PM_{2.5}$ aerosols in Queens, New York: solubility and temporal trends. Atmos. Environ. 40 (Suppl. 2), 238–251.
Riccio, A., Giunta, G., Chianese, E., 2007. The application of a trajectory classification procedure to interpret air pollution measurements in the urban area of Naples (Southern Italy). Atmos. Environ. 376 (21), 198–214.
Roland, R.D., Hess, G.D., 2004. Description of the HYSPLIT 4 Modeling System. NOAA Technical Memorandum ERL.
Schwartz, J., Dockery, D.W., Neas, L.M., 1996. Is daily mortality associated specifically with fine particles? J. Air Waste Manage. Assoc. 46 (10), 927–939.
Streets, D.G., Bond, T.C., Carmichael, G.R., Fernandes, S.D., Fu, Q., He, D., Klimont, Z., Nelson, S.M., Tsai, N.Y., Wang, M.Q., Woo, J.H., Yarber, K.F., 2003. An inventory of gaseous and primary aerosol emissions in Asia in the year 2000. J. Geophys. Res. 108 (D21).
Wang, W.H., 1990. Climate in Inner Mongolia. China Meteorological Press, Beijing (in Chinese).
Wang, J.G., 2005. Climate in Shandong. China Meteorological Press, Beijing (in Chinese).
Wang, Y.Q., Zhang, X.Y., Arimoto, R., Cao, J.J., Shen, Z.X., 2004. The transport pathways and sources of PM_{10} pollution in Beijing during spring 2001, 2002 and 2003. Geophys. Res. Lett. 31 (14), 1–4.
World Health Organization (WHO), 2006. Air Quality Guidelines for Particulate Matter, Ozone, Nitrogen Dioxide and Sulfur Dioxide Global Update 2005 Summary of Risk Assessment. http://www.who.int/phe/healthtopics/outdoorairaqg/en/index.html.
Yin, X.H., Shi, S.L., Zhang, M.Y., Li, J., 2007. Variations of dust weather in Beijing and analysis of sources of sand. Plateau Meteorol. 26 (5), 1039–1044 (in Chinese).
Zhou, Y.H., 1989. Handbook of Weather Forecast in Shanxi. China Meteorological Press, Beijing (in Chinese).